Available online at www.sciencedirect.com

ScienceDirect

IFAC Papers Online CONFERENCE PAPER ARCHIVE

IFAC PapersOnLine 55-25 (2022) 91–96

Enhanced AOCS verification techniques for Euclid's high-pointing performance ⋆

D. Navarro-Tapia * **A. Marcos** *,1 **J. Veenman** **,2

* *Technology for Aerospace Control (TASC) Ltd, 16 Stembridge, Martock, TA12 6BN, United Kingdom; (e-mail: diego.navarro-tapia/andres.marcos@tasc-group.com)*

** *SENER Aeroespacial, C/ Severo Ochoa 4, 28760 Tres Cantos, Madrid, Spain; (e-mail: joost.veenman@aeroespacial.sener)*

Abstract: This paper presents an enhanced Verification and Validation (V&V) framework accompanied by dedicated tools that allows to analytically evaluate pointing error performance of high-pointing accuracy missions in the presence of disturbances and uncertainties. The proposed analysis approach poses the V&V problem in the robust control framework using linear fractional transformation modelling theory (to include model uncertainties) and frequency dependent weighting functions (to capture the spectral properties of the disturbances and the pointing error performance metrics), and is based on the structured singular value approach as well as the integral quadratic constraint (IQC) framework. The validity of this formal approach is exemplified through the verification of the stringent pointing performance of the Euclid mission during the science observation phase. The results show that the proposed enhanced V&V approach is capable of providing certificates for robust stability and performance for all modelled uncertainties.

Keywords: Robust control, IQC, Verification and Validation, AOCS, Euclid

1. INTRODUCTION

Future satellite missions require efficient and cost effective attitude and orbital control systems (AOCS) that account, by design, for disturbance and system uncertainties. Furthermore, AOCS architectures that integrate platform and payload requirements are necessary to push performance resulting in, for example, more flexible and versatile spacecraft structures, complex system architectures, and adaptive GNC algorithms. In addition, maximizing science return involves complex mission requirements that need to be effectively validated and verified. All this calls for enhanced formal and simulation-based verification approaches accompanied by dedicated tools that offer the capability to address the involved challenges in a systematic fashion.

In the past few decades, techniques from the robust control domain as well as the management of complexities such as uncertainties, nonlinearities, and coupling in system dynamics has significantly progressed into what has become a powerful framework for the stability and performance analysis of complex uncertain control interconnections. The main goal of this paper is to present an enhanced AOCS V&V approach supported by dedicated tools that allows reducing the time and cost of performing AOCS functional verification campaigns as well as improving the quality of the AOCS pointing robustness and performance verification process. A relevant reference in this context is Sanfedino et al. (2022) where the robust control framework is applied for worst-case pointing analysis.

The proposed V&V framework relies on linear fractional transformation (LFT) theory (Doyle et al. (1991)), to effectively include plant uncertainties in the analysis. Furthermore, inspired by the research of Pittelkau and McKinley (2012), the approach allows including dedicated pointing matrices, which yield the quality of the pointing as function of variability of the spacecraft dynamics in the presence of the modelled uncertainties and external disturbances, thereby allowing to obtain a quantitative indication of robust stability and pointing performance. In this context, this paper presents new μ and integral quadratic constraint (IQC) based tools that enable the efficient analysis of such problems. The reader is referred to Veenman et al. (2021) and Veenman et al. (2016) and references therein for a more detailed exposure. The effectiveness of the tools is demonstrated on a realistic study case derived from the Euclid mission where Euclid's stringent pointing performance is verified in the presence of uncertainties and disturbances.

The paper is organised as follows. In Section 2, the robust pointing error analysis approach is presented. Section 3 briefly describes the Euclid mission and the analysis interconnection used for the subsequent science high-pointing analysis. Then, the results of the enhanced V&V approach are presented in Section 4. Finally, conclusions are given in Section 5.

⋆ This work is part of the project "Enhanced Techniques for AOCS GNC functional verification (AOCS-EV II)" funded by ESA through the contract No. 4000126163/18/NL/GLC.

[1] Dr. Marcos is also a *Beatriz Galindo* Distinguished Senior Researcher at Universidad Carlos III de Madrid (UC3M), Spain.

[2] Dr. Veenman currently provides his services to SENER Aeroespacial as senior consultant through Novantec B.V.

10.1016/j.ifacol.2022.09.329

2. ENHANCED V&V APPROACH

2.1 Pointing error analysis

The European Cooperation for Space Standarization (2008) defines performance error metrics for control systems in the frame of Space projects. A set of the most relevant ones are depicted in Fig. 1 and described next:

- Absolute Performance Error (APE): instantaneous value of the performance error at any given time;
- Relative Performance Error (RPE): difference between the APE within a time interval Δ_t and the mean value of the APE over the same time interval;
- Mean Performance Error (MPE): mean value of the APE over a specified time interval Δ_t;
- Performance Drift Error (PDE): difference between MPEs taken over two time intervals separated by a specified time Δ_{ts} within a single observation period.

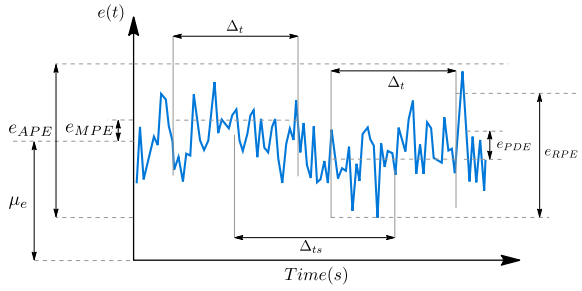

Fig. 1. Pointing error signals definition (Ott et al. (2011))

ESA's pointing error engineering handbook (see Ott et al. (2011)) provides guidelines for analysing the above pointing error indices using the closed-loop interconnection shown in Fig. 2. The interconnection consists of a control block K connected to a generalised dynamics model P, which comprises the spacecraft/payload dynamics as well as all relevant sensor and actuator models. This formulation allows analysing the dynamical properties from the disturbance inputs d to the pointing error signals e_{metric} (e.g. e_{APE},e_{RPE},...).

The pointing error analysis is based on the assumption that the disturbance inputs d and the pointing error signals e_{metric} are stationary random noise processes that follow a Gaussian distribution with zero mean. Such noise processes are well described by means of their amplitude spectral densities (ASDs). Here the input weighting function block W_{in} in Fig. 2 is selected to normalize the weighted inputs w to one, whereas the performance error signals e_{metric} are computed by weighting the output performance error e with rational functions that approximate the underlying ASD of each pointing error metric, see second column in Table 1.

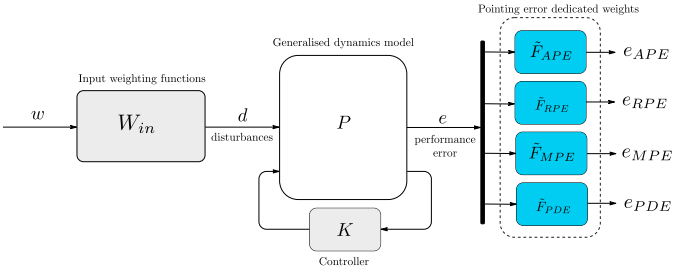

Fig. 2. Interconnection for pointing error analysis

Under the above assumptions, the transfer from weighted inputs w to the specific pointing error signal e_{metric} ($M_{w\to e_{metric}}$) is physically meaningful because it analytically describes the ASD of each pointing error signal. And more importantly, it can be used to compute the standard deviation of the pointing error signals, as shown in Eq. 1. Note that σ_{metric} also equals the $\mathcal{H}_2$ norm of the system transfer $M_{w\to e_{metric}}$.

$$\sigma_{metric} = \sqrt{\frac{1}{2\pi}\int_0^\infty |M_{w\to e_{metric}}|^2 d\omega} = ||M_{w\to e_{metric}}||_2 \tag{1}$$

The final pointing error indices are obtained by multiplying the obtained standard deviations by the applicable confidence level of the requirements (e.g. $n_p = 3$ for 99.7% probability level) and by summing the corresponding mean values μ_e (only for APE and MPE), see third column of Table 1.

2.2 Enhanced robust pointing error analysis formulation

The pointing error analysis approach is formulated in an explicit robust setting by augmenting the interconnection shown in Fig. 2 by means of LFT models that capture the system uncertainties as shown in Fig. 3. This robust framework offers a powerful framework to investigate systems under the presence of generic uncertainties.

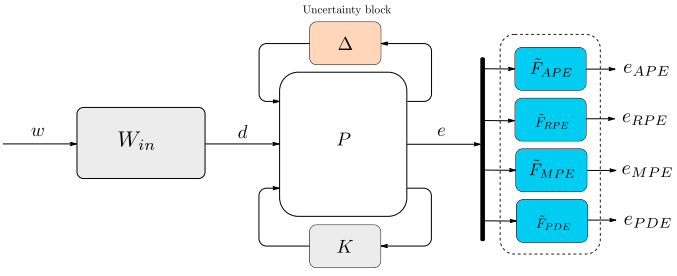

Fig. 3. Interconnection for robust pointing error analysis

Table 1. Pointing error metric evaluation

Index	Pointing error dedicated weighting functions	Pointing error metric evaluation
APE	$\tilde{F}_{APE} = 1$	$\epsilon_{APE} = n_p\sigma_{APE} + \lvert\mu_e\rvert$
RPE	$\tilde{F}_{RPE} = \frac{i\omega\Delta_t(i\omega\Delta_t+\sqrt{12})}{(i\omega\Delta_t)^2+6(i\omega\Delta_t)+12}$	$\epsilon_{RPE} = n_p\sigma_{RPE}(\Delta_t)$
MPE	$\tilde{F}_{MPE} = \frac{2(i\omega\Delta_t+6)}{(i\omega\Delta_t)^2+6(i\omega\Delta_t)+12}$	$\epsilon_{MPE} = n_p\sigma_{MPE} + \lvert\mu_e\rvert$
PDE	$\tilde{F}_{PDE} = \tilde{F}_{MPE}\frac{2i\omega\Delta_{ts}(i\omega\Delta_{ts}+6}{(i\omega\Delta_{ts})^2+6(i\omega\Delta_{ts})+12}$	$\epsilon_{PDE} = n_p\sigma_{PDE}(\Delta_t,\Delta_{ts})$

Within this setting, the structured singular value (SSV/μ) techniques allow obtaining certificates for robust stability and performance. To perform the SSV analysis, the system is augmented by an output weighting function W_{out} that translates the desired specifications in the frequency domain and normalises the system such that, if the control requirements are satisfied, then:

$$\max_{\Delta \in \mathbf{\Delta}} ||W_{out} M_{w \to e_{metric}(\Delta)}||_\infty \leq 1 \quad (2)$$

However, the above μ analysis cannot be directly applied to this case because the robust performance condition in Eq. 2 is expressed in terms of the $\mathcal{H}_\infty$ norm, whereas the pointing error requirements are generally formulated in the $\mathcal{H}_2$-norm sense (see Euclid requirements in Table 2).

In order to reconcile both metrics, the analysis is reformulated as proposed in Preda (2018). The key idea of this approach is that the $\mathcal{H}_2$-norm of any function $F(s)$ that over bounds the largest singular values of the transfer $M_{w \to e_{metric}}(\Delta)$, as illustrated in Fig. 4, will always be larger than the worst-case pointing performance $\sigma_{WCmetric}$, see Eq. 3. It is noted that F must be strictly proper to have a well-defined $\mathcal{H}_2$ norm.

$$\sigma_{WCmetric} = \max_{\Delta \in \mathbf{\Delta}} ||M_{w \to e_{metric}(\Delta)}||_2 < ||F||_2 \quad (3)$$

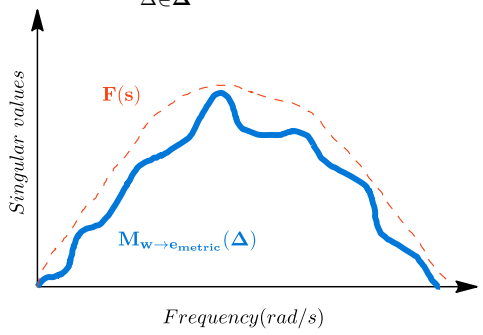

Fig. 4. Example of $F(s)$ over bounding the singular values of the transfer $M_{w \to e_{metric}}(\Delta)$

Based on the above discussion, this approach provides guarantees that the worst-case standard deviation of the metric ($\sigma_{WCmetric}$) is smaller than the $\mathcal{H}_2$-norm of F for any uncertainty within the defined LFT range $\Delta \in \mathbf{\Delta}$. In other words, the $\mathcal{H}_2$-norm of F sets an upper bound for the worst-case pointing error index. The robust performance analysis is reformulated to find a function F that accurately over-bounds the largest singular values of $M_{w \to e_{metric}}(\Delta)$. F is computed in Preda (2018) using a multi-model optimization problem. In our approach, F is efficiently computed in two steps: First, the largest singular values of the system $M_{w \to e_{metric}}(\Delta)$ are computed at each frequency by means of MATLAB's Robust Control Toolbox (Balas et al. (2005)). Then, F is obtained by fitting the obtained frequency responses to a rational function. The results presented in the sequel demonstrate the effectiveness of the procedure.

In addition to the latter approach, the interconnection shown in Fig. 3 can be also considered in the integral quadratic constraint (IQC) framework. This offers the possibility to directly compute the pointing performances using the $\mathcal{H}_2$-metric, avoiding the need to compute F altogether. In the scope of the same project, a new IQC toolbox called *IQClab* (Veenman et al., 2021) was developed that allows performing such analyses (among many other things) as further detailed in Section 4.5.

3. EUCLID SCIENCE MISSION

3.1 Euclid science mission description

Euclid is an ESA medium class cosmology mission dedicated to the investigation of Dark Energy and Dark Matter, with TASI as prime contractor and SENER Aeroespacial leading the AOCS development. The mission consists of scanning certain regions of the sky with two payload instruments: a visual instrument (VIS) and a near-infrared spectrometry instrument (NISP).

During the science observations, the spacecraft is in inertial pointing with highly stringent pointing error requirements, see Table 2. Here the visual observations have a duration of 600s, while the infrared observations last for 100s.

Table 2. Pointing error requirements for Euclid during science visual observations

	APE	RPE
x axis	$\epsilon_{APEx} = 6$ arcsec	$\epsilon_{RPEx} = 75$ mas
y axis	$\epsilon_{APEy} = 6$ arcsec	$\epsilon_{RPEy} = 75$ mas
z axis	$\epsilon_{APEz} = 21$ arcsec	$\epsilon_{RPEz} = 1500$ mas

3.2 Science-mode Euclid closed-loop interconnection

The closed-loop LFT interconnection for the Euclid science mode during science observations is depicted in Fig. 5. In order to comply with the above stringent pointing requirements, the actuation is provided by a cold-gas micro propulsion system (MPS) that can generate very small and precise torques. The MPS actuator is represented here by an LFT model with three inputs (the control commanded forces Fc_{MPS} and two disturbance inputs, bias b_{MPS} and noise n_{MPS}) and two outputs (forces and torques signals F_{MPS} and T_{MPS}). The uncertainty block Δ_{MPS} models the uncertain misalignments of the 12 MPS thrusters.

The spacecraft dynamics are embedded into the dynamic kinematic environment (DKE) LFT model, which models the uncertain sloshing dynamics as well as MCI parametric uncertainties (spacecraft mass, centre of mass and inertia).

The navigation set during science observations relies on a high performing Gyroscope sensor and the so-called Fine Guidance Sensor (FGS). The gyroscope model receives the spacecraft angular rate ω_{SC} from the DKE model and outputs the gyroscope angular rate measurements ω_{GYR}. This model includes three disturbance signals: constant bias b_{GYR}, bias instability bI_{GYR} and angular random walk noise n_{GYR}, and models the gyroscope and IMU's misalignments and the scale factor as parametric uncertainties. The fine guidance sensor model receives as inputs the spacecraft attitude θ_{SC} and the FGS noise n_{FGS}, and outputs the FGS angle θ_{FGS} in the unit sensor reference frame.

The navigation function is completed with the FGS-GYR (stationary) Kalman filter (FGKF), which combines the GYR and FGS measurements with an-board model that

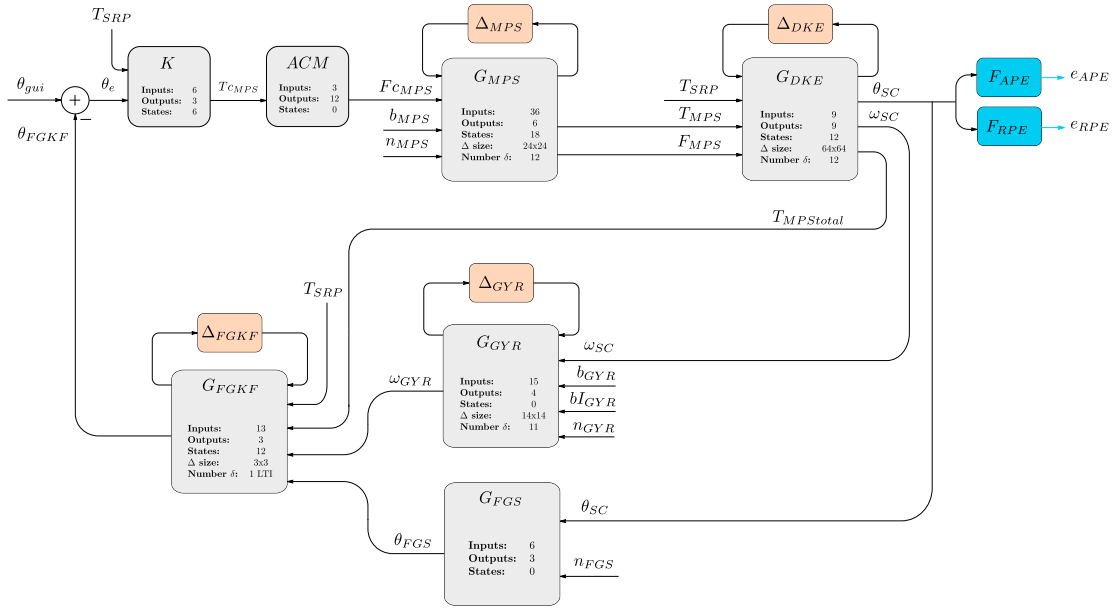

Fig. 5. Euclid closed-loop interconnection for analysis

propagates the spacecraft dynamics and MPS control commands. This LFT model captures the error of the SRP torque estimation using a dynamic LTI uncertainty block.

Finally, the control function is composed of three-axes diagonally repeated PID controller whose outputs are scaled by the estimated spacecraft inertia, while the actuator manager ACM converts the commanded torques Tc_{MPS} into individual MPS thruster forces Fc_{MPS}.

3.3 Augmented generalized plant

In preparation for the subsequent robustness analysis, all the individual models shown in Fig. 5 (i.e. GNC, actuators, sensors, and spacecraft models) are rearranged into the LFT interconnection depicted in Fig. 6, where P is the so-called generalized closed-loop plant interconnection and Δ is a diagonal block gathering the different Δ_i blocks from Fig. 5.

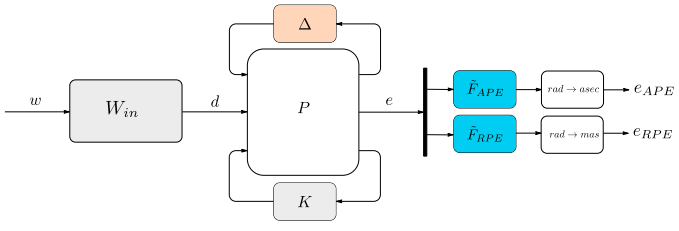

Fig. 6. Euclid augmented interconnection

The generalized closed-loop interconnection has a set of disturbance inputs d and outputs e. The inputs comprise the MPS noise and bias (n_{MPS} and b_{MPS}); SRP torque (T_{SRP}); GYR bias, bias instability and noise (b_{GYR}, bi_{GYR} and n_{GYR}); and FGS noise (n_{FGS}). At the output side, the spacecraft attitude (θ_{SC}) is pulled out to be analysed.

The input weighting function W_{in} in Fig. 6 is a diagonal block containing the individual input weights for each disturbance input. As mentioned in Section 2.1, the input weighting functions are selected to normalize the PSD of the weighted disturbance inputs w to one. Noise inputs are represented by their ASDs, whereas biases are modelled here as low-frequency stochastic signals. In particular, bias inputs are represented by a variance term σ_b^2 and a low-pass filter with very low bandwidth.

Note also that the augmented interconnection includes the rational approximation functions presented in Table 1 (both highlighted in blue) to obtain the pointing error signals e_{APE} and e_{RPE}. Also it is emphasized that the output signals are converted into adequate units to be analysed, e.g. APE in arcsec and RPE in milli-arcsec.

4. ENHANCED V&V RESULTS

This section presents the robust stability and performance analyses for the Euclid science-mode observations, focussing on the analysis of the RPE index for visual exposures.

4.1 Robust stability analysis

The SSV/μ approach is applied here to certify the robust stability properties of the closed-loop system presented in Section 3. The results provided by the μ analysis are shown in Fig. 7. The first conclusion that can be drawn from this plot is that the values of μ are smaller than one for all frequencies, implying that the system is robustly stable for all modelled uncertainties $\Delta \in \mathbf{\Delta}$. In addition, μ offers a frequency-wise insight on the stability degradation. For instance, the maximum peak of the plot (around 3 rad/s) corresponds to the sloshing dynamics of the system.

4.2 Nominal RPE performance analysis

In this subsection, the steady-state RPE performance is analysed for the nominal case ($\Delta = 0$) following the approach described in Section 2.1. The results are reported in the second column of Table 3 for the three axes. Note

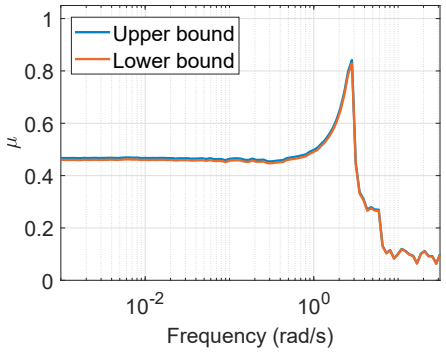

Fig. 7. Robust stability analysis

that all values are given in milli-arcsec (mas). It is clear from the table that the nominal system satisfies with margin the RPE mission specifications.

The computed nominal RPE values can be seen as predicted upper bounds for the RPE index. To evaluate this, a campaign of 100 random-seed runs using nominal conditions ($\Delta = 0$) was carried out. For this analysis, the generalized plant P was fed with the disturbance inputs from the (nonlinear) Euclid design facility and the resulting RPE signals computed. The results are given in Fig. 8, where the obtained bounds (i.e. second column of Table 3) are depicted in dash magenta lines. As can be seen the RPE variation range from the simulations is correctly predicted by the analytical RPE analysis.

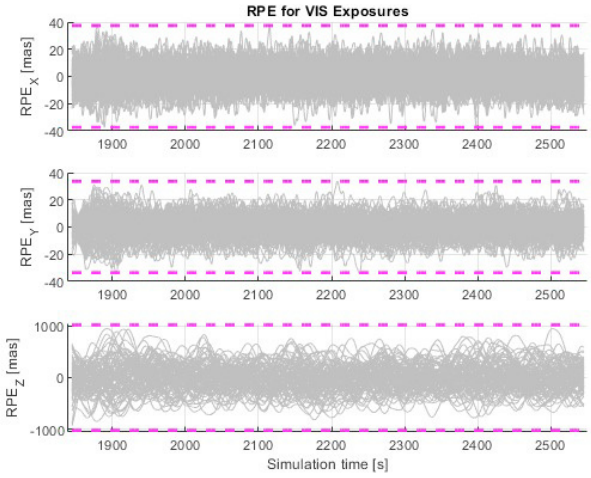

Fig. 8. RPE nominal performance validation

4.3 Robust RPE performance analysis for visual exposures

This section presents the robust performance analysis of the RPE index for the Euclid visual exposures. Recall from Section 2.2 that the robust pointing error analysis is formulated in three steps. First, the largest singular values of the system from weighted inputs w to pointing error signal e_{RPE} are computed at each frequency for the uncertainty set $\mathbf{\Delta}$, and subsequently fitted into a rational function $F(s)$ that over-bounds them. And finally, using the pointing error evaluation from Table 1, an upper bound of the worst-case RPE index can be computed as follows: $\hat{\sigma}_{WCmetric} = 3||F(s)||_2$.

The results of the robust RPE analysis are reported in the eighth column of Table 3, together with the results of two additional analyses: vertex approach, where all uncertainties in Δ are set to $+1$ and -1; and Monte Carlo approach, where the uncertainties are randomly sampled within the range $\mathbf{\Delta}$. The vertex approach provides higher and lower values than the nominal RPE levels, but fails to capture actual worst cases. The Monte Carlo approach provides higher RPE values as the number of runs is increased, but there are no guarantees that a worst case is found by running more cases. On the other hand, the robust RPE approach proposed in this paper provides non-conservative steady-state results with guarantees. The results also allows to infer that the RPE specifications are satisfied for any uncertainty within the range $\Delta \in \mathbf{\Delta}$.

4.4 Sensitivity analyses

The proposed V&V approach also allows to study the degradation of the worst-case RPE index due to system uncertainties. Fig. 9 shows this sensitivity analysis for the x-axis, where the results are provided against a normalized uncertainty amount (being 0 the nominal level, and 1 the uncertainty range $\mathbf{\Delta}$). As can be seen, the system is quite robust against the modelled uncertainties, since the RPE metric requirement is satisfied for almost 30 times the uncertainty size defined for the mission.

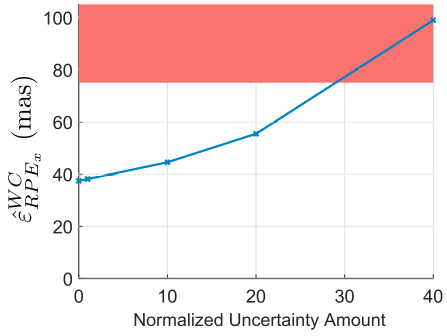

Fig. 9. Sensitivity analysis for increasing uncertainty size

A second sensitivity analysis is performed to study the degradation of the worst-case x-axis RPE index for increasing sensor and actuator noise levels, see Fig. 10. The results allow to predict that the RPE requirement is violated when noise levels are increased by nearly 100%. Thus, the system shows sufficient robustness against uncertain noise levels.

Table 3. RPE index analysis

Axis	Nominal	Vertex		Monte Carlo			Robust RPE	Constraint (mas)
	$3\|\|M_{w\to e_{RPE}}(\Delta=0)\|\|_2$	all $\delta_i=-1$	all $\delta_i=+1$	100 runs	1000 runs	10000 runs	$3\|\|F(s)\|\|_2$	
x axis	37.46	37.63	37.31	37.81	37.88	37.92	38.1	< 75
y axis	33.57	33.63	33.51	34.24	34.25	34.32	35.06	< 75
z axis	1017.2	1013.82	1020.55	1020.4	1020.55	1020.59	1021.24	< 1500

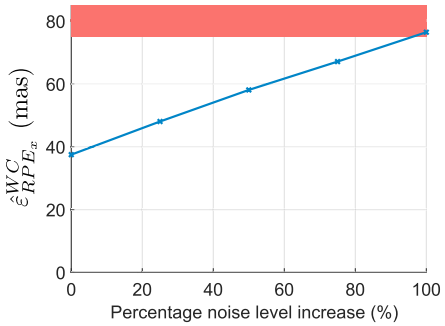

Fig. 10. Sensitivity analysis for increasing noise levels

4.5 IQC-analysis results

As mentioned earlier, the robustness analysis can also be performed using our new toolbox *IQClab*, which supports the direct verification of the $\mathcal{H}_2$-metric and hence simplifies the procedure described in Section 2.2 at the cost of a higher computational load. To demonstrate this, this section repeats the RPE sensitivity analysis for increasing noise levels performed in Section 4.4.

Just as for to the SSV approach, the IQC-analysis considers the augmented interconnection in Fig. 6. First, an LFT model order reduction is performed with the aim to reduce the computational load of the analysis. Subsequently, the analysis is performed by capturing the modelled uncertainties using so-called DG multipliers and setting the performance index to the $\mathcal{H}_2$-norm. For reasons of space, the reader is referred to Veenman et al. (2021) as well as *www.iqclab.eu* for further details on the usage of *IQClab*.

The results are shown in Fig. 11. Again, the noise levels remain well within their requirements up to 62%, 63%, 40% for the x, y, and z-axis respectively. These values are somewhat more conservative if compared to the robustness analysis in Section 4.4. This gap can potentially be reduced by choosing higher order IQC-multipliers at the cost of more computational load. Nevertheless, the analysis reveals that the robust steady state RPE pointing performances are well within the given requirements.

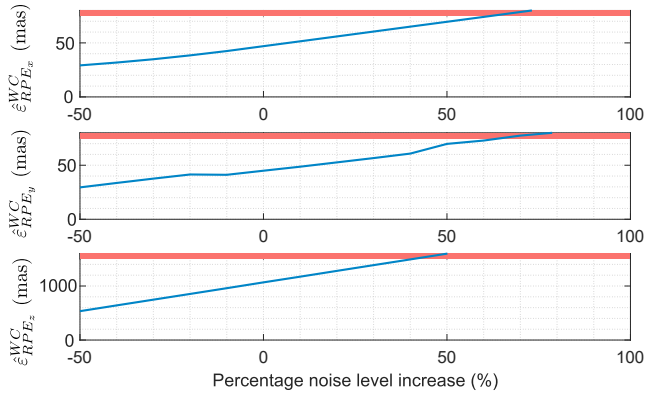

Fig. 11. IQC-based analysis for increasing noise levels

5. CONCLUSION

In this paper we have presented a systematic approach supported by dedicated tools for the analysis of complex uncertain AOCS pointing systems, which are capable of providing certificates for robust stability and pointing performance in the presence of model uncertainties. The proposed framework and tools rely on the LFT modelling theory and dedicated frequency-dependent pointing functions to describe the quality of the pointing as a function of the variability of the spacecraft dynamics in the presence of stochastic disturbance inputs and uncertainties.

The enhanced V&V approach was exemplified through the verification of the stringent pointing performance of the Euclid mission during the science observations. It was demonstrated that the Euclid closed-loop system is robustly stable for all modelled uncertainties, and that the RPE requirements are well satisfied even in the presence of uncertainties and increased noise levels. The results reveal that the proposed framework is effective in providing detailed insights on the robustness of a system. This enables the early detection of potential design flaws and could reduce the time needed for typically time consuming Monte Carlo campaigns.

ACKNOWLEDGEMENTS

The authors would like to thank Valentin Preda and Samir Bennani (ESA-ESTEC), Carlos Ardura (SENER Aeroespacial), Fabrice Boquet, and Bénédicte Girouart (ESA-ESTEC, technical officers) for their valuable support, guidance, and feedback in the project.

REFERENCES

Balas, G.J., Chiang, R., Packard, A., and Safonov, M.G. (2005). *Robust Control Toolbox*. The MathWorks, Inc.

Doyle, J.C., Packard, A., and Zhou, K. (1991). Review of LFTs, LMIs, and μ. In *Proceedings of the* 30^{th} *IEEE Conference on Decision and Control*, 1227–1232.

European Cooperation for Space Standarization (2008). Pointing performance standard ECSS-E-ST-60-10C. In *ESA-ESTEC Requirements and Standards Division*.

Ott, T., Benoit, A., van den Braembussche, W., and Fichter, W. (2011). ESA pointing error engineering handbook. In 8^{th} *International ESA Conference on Guidance, Navigation & Control Systems, 2011*.

Pittelkau, M. and McKinley, W. (2012). Pointing error metrics: Displacement, smear, jitter, and smitter with application to image motion mtf. In *AIAA/AAS Astrodynamics Specialist Conference*.

Preda, V. (2018). *Robust microvibration control and worst-case analysis for high pointing stability space missions*. Ph.D. thesis, Université de Bordeaux.

Sanfedino, F., Alazard, D., Preda, V., and Oddenino, D. (2022). Integrated modeling of microvibrations induced by solar array drive mechanism for worst-case end-to-end analysis and robust disturbance estimation. *Mechanical Systems and Signal Processing*, 163.

Veenman, J., Scherer, C.W., Ardura, C., Bennani, S., Preda, V., and Girouart, B. (2021). IQClab: a new IQC based toolbox for robustness analysis and control design. In 4^{th} *IFAC Workshop on Linear Parameter Varying Systems, 2021*.

Veenman, J., Scherer, C.W., and Koroglu, H. (2016). Robust stability and performance analysis based on integral quadractic constraints. *European Journal of Control*, 31, 1–32.